Struct Multidisc Optim (2012) 46:327–342
DOI 10.1007/s00158-012-0781-9

RESEARCH PAPER

Phase-field based topology optimization with polygonal elements: a finite volume approach for the evolution equation

Arun L. Gain · Glaucio H. Paulino

Received: 12 October 2011 / Revised: 5 January 2012 / Accepted: 6 February 2012 / Published online: 3 April 2012

Abstract Uniform grids have been the common choice of domain discretization in the topology optimization literature. Over-constraining geometrical features of such spatial discretizations can result in mesh-dependent, sub-optimal designs. Thus, in the current work, we employ unstructured polygonal meshes constructed using Voronoi tessellations to conduct structural topology optimization. We utilize the phase-field method, derived from phase transition phenomenon, which makes use of the Allen-Cahn differential equation and sensitivity analysis to update the evolving structural topology. The solution of the Allen-Cahn evolution equation is accomplished by means of a centroidal Voronoi tessellation (CVT) based finite volume approach. The unstructured polygonal meshes not only remove mesh bias but also provide greater flexibility in discretizing complicated (e.g. non-Cartesian) domains. The features of the current approach are demonstrated using various numerical examples for compliance minimization and compliant mechanism problems.

Keywords Topology optimization · Polygonal finite elements · Voronoi tessellation · Phase-field method · Allen–Cahn equation

A. L. Gain · G. H. Paulino (✉)
Department of Civil and Environmental Engineering,
University of Illinois at Urbana-Champaign,
205 N. Mathews Ave., Urbana,
IL 61801, USA
e-mail: paulino@uiuc.edu

1 Introduction

Topology optimization has emerged as a popular technique for structural optimization which deals with distribution of material in a given domain with variable connectivity so as to satisfy certain design objectives. In manufacturing industries, topology optimization is often used as a tool to obtain preliminary conceptual designs. Some of the early works include Bendsøe and Kikuchi (1988) and Suzuki and Kikuchi (1991), in which the homogenization method was used to determine macroscopic structure properties, such as elastic modulus, based on the microstructure configuration. Subsequently, its variant, such as the Solid Isotropic Material with Penalization (SIMP) method, was proposed (Bendsøe 1989; Rozvany et al. 1992; Bendsøe and Sigmund 1999), which provided a simple approach to determine intermediate material densities.

Recently, a new set of approaches for topology optimization have emerged which use implicit functions rather than explicit parameterization, as illustrated by Fig. 1. The level-set method is one such approach (Osher and Sethian 1988; Sethian 1999; Osher and Fedkiw 2003) that uses the Hamilton–Jacobi equation to track fronts and free boundaries. Allaire and Jouve (2004), Wang et al. (2003), among others, explored the application of level-sets in shape and topology optimization. Since its inception, it has been applied in a variety of fields such as fluid mechanics (Pingen et al. 2010) and image processing (Osher and Fedkiw 2003). In general, level-set functions become too flat or too steep during the course of evolution and thus, for numerical accuracy, they need to be reinitialized periodically, for example, to a signed distance function.

In order to avoid the need for reinitialization, which can be costly, another implicit function approach has come forth, known as the phase-field method. It has been widely

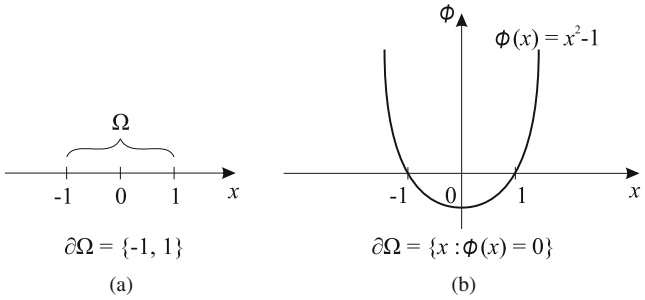

Fig. 1 Explicit (**a**) versus implicit (**b**) representation

used in the field of materials science as a means to study phase transition phenomenon. For instance, it is especially suitable to investigate the stability of systems with multiple unstable phases. Cahn and Hillard (1958) and Allen and Cahn (1979) used the theory of phase transition to study liquid phases with variable densities. *In essence, the phase-field method is a diffuse interface model where the boundary between phases is not sharp, but considered to have a finite thickness, thus providing a smooth transition for the physical quantities between the phases.* In the phase-field method, explicit interface tracking is avoided and topologies are evolved by solving the governing equations over the complete design domain without prior information about the location of phase interfaces. Caginalp (1986) provided a mathematical analysis of the phase transition method. Contrary to the traditional phase-field approach with finite thickness diffuse interfaces, Sun and Beckermann (2007) presented an advection equation based phase-field method which explicitly defines and tracks sharp interfaces. In the technical literature, the phase-field method has been used in a wide variety of fields such as fracture mechanics (Aranson et al. 2000), visual reconstruction (March 1992), and crystal growth simulations (Kobayashi 1993).

The phase-field method is especially attractive and suitable for topology optimization (Bourdin and Chambolle 2003). Wang and Zhou (2004a) used van der Waals-Cahn-Hillard phase transition theory to propose a phase-field method for topology optimization by considering a design domain consisting of bi-material phases of solids. Later they extended the approach to three-phase systems (Wang and Zhou 2004b). Burger and Stainko (2006) introduced a phase-field based relaxation scheme for structural topology optimization problems with local stress constraints. Zhou and Wang (2007) used the Cahn-Hilliard theory and the multi-grid method to study minimum compliance problems. Recently, Takezawa et al. (2010) utilized a time dependent reaction-diffusion equation, known as Allen–Cahn equation (Allen and Cahn 1979), for the evolution of topologies in a structural optimization problem. With a suitable choice of double well potential function, the evolution equation can be approximately represented as a conventional steepest decent method. Also, Wallin et al. (2011) presented a topology optimization procedure which uses a volume preserving Cahn-Hillard model and an adaptive finite element formulation.

For simplicity, topology optimization problems are often solved on Cartesian meshes. The orientation of members in the evolving topologies are thus biased because of the geometrical constraints of such meshes. Accurate representation of general design domains and boundary conditions requires additional effort. Moreover, it is well known that traditional density based topology optimization on Cartesian meshes suffer from numerical artifacts such as checkerboard patterns and one-node connections (Diaz and Sigmund 1995; Sigmund and Peterson 1998). Techniques such as filters (Sigmund and Peterson 1998; Bourdin 2001; Guest et al. 2004) may alleviate numerical anomalies and mesh bias. However, Rozvany et al. (2003) indicated that such heuristic schemes can result in (considerable) weight increase. Polygonal elements address some of the aforementioned problems. They not only provide convenience and flexibility in discretizing complicated design domains but also lead to optimal designs that are not biased by the mesh discretization. For instance, polygonal elements alleviate one-node connection problems and prevent checkerboard pattern from occurring in density methods (Talischi et al. 2010). The Voronoi diagram has been a popular choice for generating polygonal meshes in the field of computer graphics, robotics, pattern recognition, etc (Ghosh and Mukhopadhyay 1991; Ghosh 2011) and is the method of choice in this work.

In this paper, we utilize unstructured polygonal meshes, constructed using Voronoi tessellations, for structural topology optimization employing the phase-field method. In order to evolve the partial differential equation (PDE), known as the Allen–Cahn equation, a centroidal Voronoi tessellation based finite volume approach (Vasconcellos and Maliska 2004) is used. We also present a heuristic finite difference approach, as an alternate scheme, which can be used for assessing the accuracy of results obtained from the finite volume approach. To generate polygonal meshes, we use `PolyMesher` (Talischi et al. 2011), which is an extension of the work by Bolander and Saito (1998) and Yip et al. (2005).

The remainder of this paper is organized as follows. In Section 2, we discuss the formulation for the topology optimization problem followed by a review of the polygonal finite element method. Section 3 reviews the phase-field method and addresses the finite volume and finite difference approaches for solving the Allen–Cahn equation on non-Cartesian domains discretized using unstructured polygonal meshes. Section 4 provides several numerical examples. Finally, we conclude with some remarks in Section 5.

2 Basic formulation

The linearized elastic system considered in this work is defined as follows:

$$\begin{aligned} \nabla \cdot (\boldsymbol{C}\boldsymbol{\varepsilon}(\boldsymbol{u})) &= \boldsymbol{f} \qquad \text{in } \Omega, \\ \boldsymbol{u} &= \boldsymbol{0} \qquad \text{on } \Gamma_{\mathrm{D}}, \\ (\boldsymbol{C}\boldsymbol{\varepsilon}(\boldsymbol{u})) \cdot \boldsymbol{n} &= \boldsymbol{g} \qquad \text{on } \Gamma_{\mathrm{N}}. \end{aligned} \tag{1}$$

The bounded open set $\Omega \subset \mathbf{R}^2$ is composed of a linear isotropic elastic material with elasticity tensor $\boldsymbol{C}$. The boundary of Ω consists of two disjoint components, $\partial\Omega = \Gamma_{\mathrm{D}} \cup \Gamma_{\mathrm{N}}$, with Dirichlet-type boundary conditions on Γ_{D}, and Neumann-type boundary conditions on Γ_{N}. Here $\boldsymbol{\varepsilon}$ and $\boldsymbol{u}$ represent the linearized strain and displacement fields, respectively. Moreover, $\boldsymbol{f}$ is the body force, and $\boldsymbol{g}$ represents the surface loads. The finite element method is used to solve the above elastic system.

2.1 Topology optimization

In this work, we shall concentrate on two classes of problems, compliance minimization and linear compliant mechanisms. The first class is the compliance minimization problem. Compliance, which is work done by the loads, is given by:

$$\begin{aligned} J_1(\phi) &= \int_{\Omega} \boldsymbol{f} \cdot \boldsymbol{u}\, d\Omega + \int_{\Gamma_{\mathrm{N}}} \boldsymbol{g} \cdot \boldsymbol{u}\, d\Gamma \\ &= \int_{\Omega} \boldsymbol{C}(\phi)\boldsymbol{\varepsilon}(\boldsymbol{u}) \cdot \boldsymbol{\varepsilon}(\boldsymbol{u})\, d\Omega \end{aligned} \tag{2}$$

where ϕ is the phase-field function. The topology optimization problem of compliance minimization refers to finding the stiffest configuration under applied loads and boundary conditions.

The second class of problems addresses the design of linear compliant mechanisms. The task of the optimization problem is to maximize the displacement u_{out} performed on the specimen modeled by a spring with stiffness k_{out} (cf. Fig. 2.18 in the book by Bendsøe and Sigmund 2003). The magnitude of k_{out} controls the output displacement amplification. Thus, the linear compliant mechanism problem is written as:

$$J_2(\phi) = -u_{\mathrm{out}}(\phi) \tag{3}$$

For nontrivial solutions, we impose a volume constraint:

$$P(\phi) = \int_{\Omega} \phi\, d\Omega \tag{4}$$

on the problems (2) and (3) using the Lagrange multiplier method to obtain the following unconstrained optimization problem:

$$\inf_{\phi} \bar{J}(\phi) = J_i(\phi) + \lambda P(\phi) \qquad \text{for } i = 1, 2 \tag{5}$$

where λ is a positive Lagrange multiplier.

2.2 Polygonal finite elements

In the literature, often uniform grids of linear quads/triangles (2D) or bricks/tetrahedra (3D) are used for topology optimization problems. Because of their intrinsic geometrical constraints, such spatial discretizations bias the orientation of members and hence can result in mesh-dependent, sub-optimal designs (cf. Fig. 21 in Talischi et al. 2010). In the current work, we use polygonal meshes constructed using Voronoi tessellations (Ghosh and Mukhopadhyay 1991; Talischi et al. 2010, 2011; Ghosh 2011) to implement the phase-field method. The use of such unstructured meshes not only circumvents mesh bias but also provides greater flexibility in discretizing complicated domains (as demonstrated later) with accurate representation of boundary conditions.

We use Voronoi diagrams to generate polygonal meshes. In this approach, the given design domain with smooth boundaries is first populated with a set of random points/seeds. Using the concept of signed distance function, a set of points are generated which are the reflections of the seeds, lying near the boundary, about the boundary. The Voronoi diagram is generated for the set of random seeds and their reflections. The Voronoi cells corresponding to the random seeds represent the discretized design domain. The Voronoi diagram is forced to be centroidal in order to generate high quality meshes. The Lloyd's algorithm (Lloyd 1982) is used for the construction of centroidal Voronoi tessellations (CVTs). For more details on the polygonal mesh generation scheme, the reader is referred to Talischi et al. (2010, 2011). It should also be noted that due to the random placement of seeds, the node and element numbering will be random, resulting in a stiffness matrix of large bandwidth. If needed, the heuristic reverse Cuthill-McKee (RCM) (Cuthill and McKee 1969) algorithm is used to reduce the bandwidth of the stiffness matrix. Other equivalent algorithms can also be employed (Paulino et al. 1994a, b).

In this work, we use the natural neighbor scheme based Laplace interpolants to construct finite element shape functions for the polygonal elements (Sukumar and Tabarraei 2004). Here we briefly review the finite element scheme for convex polygons. Two points are natural neighbors of each other if they have a common Voronoi edge. Consider a point

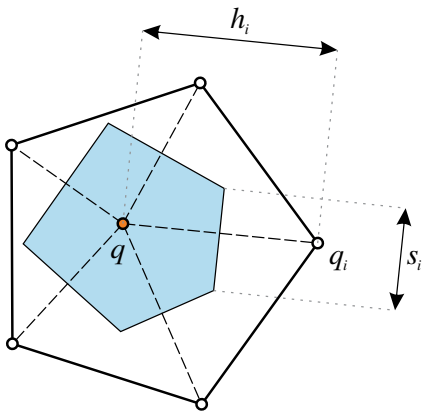

Fig. 2 Definition of the Laplace shape function. The parameter s_i denotes the length of the common Voronoi edge associated with q and q_i, and h_i is the distance between q and q_i

q and let the set of nodes $\mathcal{Q} = \{q_1, q_2, ..., q_n\}$ be its natural neighbors. The Laplace shape function for the node q_i is given by:

$$N_i(\boldsymbol{x}) = \frac{\alpha_i(\boldsymbol{x})}{\sum_{\mathcal{Q}} \alpha_j(\boldsymbol{x})}, \qquad \alpha_i(\boldsymbol{x}) = \frac{s_i(\boldsymbol{x})}{h_i(\boldsymbol{x})}, \qquad \boldsymbol{x} \in \mathbf{R}^2 \quad (6)$$

where $\boldsymbol{x}$ is the location of q, $\alpha_i(\boldsymbol{x})$ is Laplace weight function, $s_i(\boldsymbol{x})$ is the length of the common Voronoi edge associated with q and q_i, and $h_i(\boldsymbol{x})$ is the distance between q and q_i (Fig. 2).

These shape functions satisfy all the desirable properties in the context of a conforming Galerkin approximation such as non-negativity, Kronecker-delta property, and partition of unity:

$$0 \leq N_i(\boldsymbol{x}) \leq 1, \qquad N_i\left(\boldsymbol{x}_j\right) = \delta_{ij}, \qquad \sum_{\mathcal{Q}} N_i(\boldsymbol{x}) = 1 \quad (7)$$

Here, $\boldsymbol{x}_j$ represents the location of node q_j. These functions are also linearly precise or complete:

$$\sum_{\mathcal{Q}} \boldsymbol{x}_i N_i(\boldsymbol{x}) = \boldsymbol{x} \quad (8)$$

which indicates that a linear function is represented exactly by these shape functions. Furthermore, on the boundary of the domain, the Laplace shape functions are linear which along with Kronecker-delta property ensures that linear essential boundary conditions can be imposed.

3 Phase-field method

Recently, phase-field methods have been used for structural topology optimization. In the current work, we employ the approach proposed in Takezawa et al. (2010). In this method, the working domain D is considered to be composed of two phases Ω_1, Ω_0 and the boundary between the phases, ξ, which is called the diffuse interface (Fig. 3). The diffuse interface is represented by a function which interpolates between the two phases. The working domain D contains all the admissible shapes Ω, i.e., $\Omega \subset D$. Here $\Omega \subset (\Omega_1 \cup \xi)$. Thus, the phase-field function ϕ is defined as:

$$\begin{cases} \phi = 1 & \boldsymbol{x} \in \Omega_1, \\ 0 < \phi < 1 & \boldsymbol{x} \in \xi, \\ \phi = 0 & \boldsymbol{x} \in \Omega_0. \end{cases} \qquad \text{Diffuse interface} \quad (9)$$

The solid phase Ω_1 is filled with material having elasticity tensor $\boldsymbol{C}$ and the region Ω_0, which mimics a void, is filled with elasticity tensor $k_{\min}\boldsymbol{C}$. Here $k_{\min}$ is arbitrarily chosen

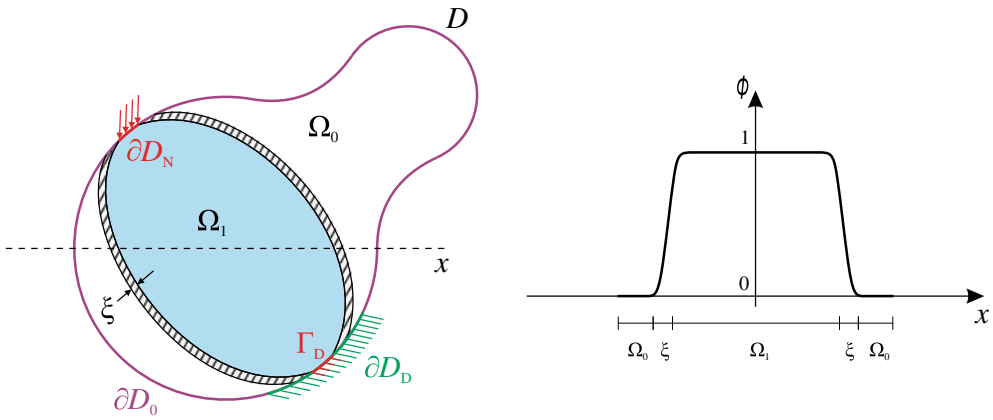

Fig. 3 Phase-field function domain. The working domain D consists of all admissible Ω. Its boundary ∂D consists of ∂D_{D} (Dirichlet-type boundary), ∂D_{N} (non-homogeneous Neumann-type boundary) and ∂D_0 (homogeneous Neumann-type boundary). Dirichlet-type boundary conditions for Ω are applied on Γ_{D}. The parameters Ω_1, Ω_0 and ξ represent solid phase, void phase and diffuse interface, respectively. Here $\Omega \subset (\Omega_1 \cup \xi)$ and ϕ is the phase-field function

to be 10^{-4}. The effective elasticity tensor $\boldsymbol{C}^*$ for the entire design domain, shown in Fig. 3, is obtained as:

$$\boldsymbol{C}^*(\phi) = \left[k_{\min} + (1 - k_{\min})\,\phi^p\right]\boldsymbol{C} \tag{10}$$

In the current study, the penalization parameter, p, is set to 3 for all numerical examples. The scheme is similar to the SIMP method (Note that $p = 3$ is also in the range $p \geq 3$ recommended in the SIMP model). Using the above definition of effective elasticity tensor, the elasticity equations (1) for the state $\boldsymbol{u}$ are extended to the entire working domain D as shown below:

$$\begin{aligned}
\boldsymbol{\nabla}\cdot\left(\boldsymbol{C}^*\boldsymbol{\varepsilon}(\boldsymbol{u})\right) &= \boldsymbol{f} \qquad \text{in } D,\\
\boldsymbol{u} &= \boldsymbol{0} \qquad \text{on } \partial D_{\mathrm{D}},\\
\left(\boldsymbol{C}^*\boldsymbol{\varepsilon}(\boldsymbol{u})\right)\cdot\boldsymbol{n} &= \boldsymbol{g} \qquad \text{on } \partial D_{\mathrm{N}},\\
\left(\boldsymbol{C}^*\boldsymbol{\varepsilon}(\boldsymbol{u})\right)\cdot\boldsymbol{n} &= \boldsymbol{0} \qquad \text{on } \partial D_0.
\end{aligned} \tag{11}$$

The boundary of the working domain ∂D consists of three disjoint components, $\partial D = \partial D_{\mathrm{D}} \cup \partial D_0 \cup \partial D_{\mathrm{N}}$, where ∂D_{D}, ∂D_0, and ∂D_{N} correspond to Dirichlet-type boundary conditions, homogeneous Neumann-type boundary conditions, and non-homogeneous Neumann-type boundary conditions with $\boldsymbol{g} \neq \boldsymbol{0}$, respectively. For all the examples in this study, the body force $\boldsymbol{f} = \boldsymbol{0}$. Also, the original design Ω is constrained to satisfy, $\Gamma_{\mathrm{N}} = \partial D_{\mathrm{N}} \cup \Gamma_0$ and $\Gamma_{\mathrm{D}} \subset \partial D_{\mathrm{D}}$. Γ_0 corresponds to the boundary of Ω with homogeneous Neumann boundary conditions.

The phases evolve over time based on the Allen–Cahn equation (reaction-diffusion equation), given by:

$$\frac{\partial\phi}{\partial t} = \kappa\boldsymbol{\nabla}^2\phi - f'(\phi), \qquad \frac{\partial\phi}{\partial\boldsymbol{n}} = 0 \text{ on } \partial D \tag{12}$$

where κ is the diffusion coefficient, and $f(\phi)$ is a double well potential function. The optimization proceeds in the direction which minimizes the design objective if $f(\phi)$ is chosen such that it satisfies the conditions (refer to Fig. 4):

$$f(0) = 0, \quad f(1) = \eta\frac{\bar{J}'(\phi_t)}{\left\|\bar{J}'(\phi_t)\right\|}, \quad \text{and} \quad f'(0) = f'(1) = 0 \tag{13}$$

where η is a scaling constant. One such $f(\phi)$ is given by:

$$f(\phi) = \frac{1}{4}\phi^2(1-\phi)^2 + \eta\frac{\bar{J}'(\phi_t)}{\left\|\bar{J}'(\phi_t)\right\|}\left(6\phi^5 - 15\phi^4 + 10\phi^3\right) \tag{14}$$

where $\bar{J}'(\phi_t)$ represents the sensitivity of the reformulated objective function $\bar{J}$ with respect to ϕ at time t. Sensitivity analysis of objective functions, such as (2) and (3), is available in the book by Bendsøe and Sigmund (2003). Thus, the Allen–Cahn equation (12) reduces to:

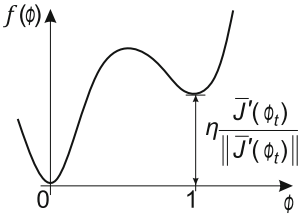

Fig. 4 Illustration of double well potential function. Here $f(\phi)$ is the double well potential function, $\bar{J}'(\phi_t)$ represents the sensitivity of the reformulated objective function with respect to ϕ at time t and η is a scaling constant

$$\frac{\partial\phi}{\partial t} = \kappa\boldsymbol{\nabla}^2\phi + \phi(1-\phi) \times\left[\phi - \frac{1}{2} - 30\eta\frac{\bar{J}'(\phi_t)}{\left\|\bar{J}'(\phi_t)\right\|}\phi(1-\phi)\right] \tag{15}$$

The evolution equation (15) can be regarded as a modified version of the steepest decent method (Takezawa et al. 2010). The phase ϕ evolves in the direction of the negative gradient of the objective function thus minimizing the objective function. We next discuss two approaches, CVT-based finite volume method and finite difference method, to solve (15) on unstructured meshes.

3.1 CVT-based finite volume (FV) method for unstructured meshes

The finite volume (FV) method is a popular method of choice for solving PDEs when dealing with unstructured grids. We employ a scheme similar to that of Vasconcellos and Maliska (2004) who proposed a centroidal Voronoi tessellation (CVT) based finite volume method for fluid flow. Consider a point p and let the set of points $\mathcal{P} = \{p_1, p_2, \ldots, p_n\}$ be its natural neighbors. The integral form of (12), over time t and on each Voronoi cell D_p, can be expressed as:

$$\int_{t,D_p}\frac{\partial\phi}{\partial t}dtdD = \int_{t,\Gamma_p}\kappa\boldsymbol{\nabla}\phi\cdot\boldsymbol{n}dtd\Gamma - \int_{t,D_p}f'(\phi)\,dtdD \tag{16}$$

Each term in (16) can be integrated as shown below (also refer to Fig. 5). First,

$$\int_{t,D_p}\frac{\partial\phi}{\partial t}dtdD = \int_{D_p}(\phi^{n+1} - \phi^n)dD \approx (\phi_p^{n+1} - \phi_p^n)V_p \tag{17}$$

where ϕ_p^n is the value of ϕ for the nth iteration at the center of the Voronoi cell corresponding to point p and V_p

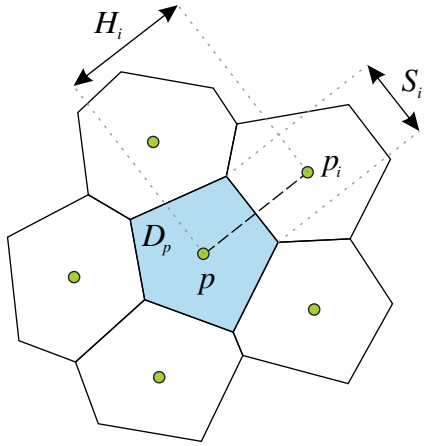

Fig. 5 Illustration of the CVT-based finite volume scheme. The parameter S_i represents the length of the common Voronoi edge associated with points p and p_i, and H_i denotes the distance between the points p and p_i

represents the area of the control volume, in the form of Voronoi cell, centered at p. Next,

$$\int_{t,\Gamma_p} \kappa \nabla\phi \cdot \boldsymbol{n} dt d\Gamma \approx \int_t \sum_{\mathcal{P}} \left[\kappa \nabla\phi^n \cdot nS\right]_i dt = \left(\sum_{\mathcal{P}} \left[\left(\kappa \frac{\partial \phi^n}{\partial \boldsymbol{n}}\right)_{p,p_i} S_i\right]\right) \Delta t = P_3 \tag{18}$$

where S_i is the length of the common Voronoi edge associated with points p and p_i. The directional derivative $(\partial\phi^n/\partial \boldsymbol{n})_{p,p_i}$ can be calculated taking advantage of the local orthogonality property of Voronoi cells:

$$\left(\frac{\partial \phi^n}{\partial \boldsymbol{n}}\right)_{p,p_i} = \frac{\phi^n_{p_i} - \phi^n_p}{H_i} \tag{19}$$

where H_i is the distance between points p and p_i. Because an explicit scheme forces the function ϕ to diverge when $\phi \notin [0, 1]$, we use a semi-implicit method to simplify the final term in (16) as shown below (Warren et al. 2003):

$$\int_{t,D_p} f'(\phi)\, dt dD \approx V_p \Delta t f'\left(\phi^n_p\right) = V_p \Delta t \begin{cases} \phi^{n+1}_p \left(1-\phi^n_p\right) r\left(\phi^n_p\right) & \text{for } r\left(\phi^n_p\right) \le 0 \\ \phi^n_p \left(1-\phi^{n+1}_p\right) r\left(\phi^n_p\right) & \text{for } r\left(\phi^n_p\right) > 0 \end{cases} \tag{20}$$

where

$$r\left(\phi^n_p\right) = \phi^n_p - \frac{1}{2} - 30\eta \frac{\bar{J}'(\phi_t)}{\left\|\bar{J}'(\phi_t)\right\|} \phi^n_p \left(1-\phi^n_p\right) \tag{21}$$

The semi-implicit FV updating scheme for ϕ in (12) can thus be expressed as:

$$\phi^{n+1}_p = \begin{cases} \dfrac{V_p \phi^n_p + P_3}{V_p\left(1-\left(1-\phi^n_p\right) r\left(\phi^n_p\right) \Delta t\right)} & \text{for } r\left(\phi^n_p\right) \le 0 \\ \dfrac{V_p \phi^n_p \left(1 + r\left(\phi^n_p\right) \Delta t\right) + P_3}{V_p\left(1+\phi^n_p r\left(\phi^n_p\right) \Delta t\right)} & \text{for } r\left(\phi^n_p\right) > 0 \end{cases} \tag{22}$$

3.2 A finite difference (FD) method on unstructured meshes

Another method to solve the Allen–Cahn equation is the finite difference (FD) scheme. As before, a semi-implicit scheme is used to discretize the reaction term. The discretized evolution equation on a structured grid follows:

$$\frac{\phi^{n+1}_{i,j} - \phi^n_{i,j}}{\Delta t} = \kappa\left(\frac{\phi^n_{i-1,j} - 2\phi^n_{i,j} + \phi^n_{i+1,j}}{(\Delta x)^2} + \frac{\phi^n_{i,j-1} - 2\phi^n_{i,j} + \phi^n_{i,j+1}}{(\Delta y)^2}\right) + \begin{cases} \phi^{n+1}_{i,j}\left(1-\phi^n_{i,j}\right) r\left(\phi^n_{i,j}\right) & \text{for } r\left(\phi^n_{i,j}\right) \le 0 \\ \phi^n_{i,j}\left(1-\phi^{n+1}_{i,j}\right) r\left(\phi^n_{i,j}\right) & \text{for } r\left(\phi^n_{i,j}\right) > 0 \end{cases} \tag{23}$$

where

$$r\left(\phi^n_{i,j}\right) = \phi^n_{i,j} - \frac{1}{2} - 30\eta \frac{\bar{J}'(\phi_t)}{\left\|\bar{J}'(\phi_t)\right\|} \phi^n_{i,j}\left(1-\phi^n_{i,j}\right) \tag{24}$$

Here Δx and Δy are the distances between grid points in the x and y direction, respectively and $\phi^n_{i,j}$ is the value ϕ for the nth iteration at the grid point $\boldsymbol{x}_{i,j}$. Thus, the scheme to update ϕ using the semi-implicit FD scheme is as follows:

$$\phi^{n+1}_{i,j} = \begin{cases} \dfrac{\phi^n_{i,j} + \Delta t\,(P_1+P_2)\kappa}{1-\left(1-\phi^n_{i,j}\right) r\left(\phi^n_{i,j}\right) \Delta t} & \text{for } r\left(\phi^n_{i,j}\right) \le 0 \\ \dfrac{\phi^n_{i,j}\left(1+r\left(\phi^n_{i,j}\right) \Delta t\right) + \Delta t\,(P_1+P_2)\kappa}{1+\phi^n_{i,j} r\left(\phi^n_{i,j}\right) \Delta t} & \text{for } r\left(\phi^n_{i,j}\right) > 0 \end{cases} \tag{25}$$

where

$$P_1 = \frac{\phi^n_{i-1,j} - 2\phi^n_{i,j} + \phi^n_{i+1,j}}{(\Delta x)^2}, \qquad P_2 = \frac{\phi^n_{i,j-1} - 2\phi^n_{i,j} + \phi^n_{i,j+1}}{(\Delta y)^2} \tag{26}$$

Polygonal meshes are unstructured in nature, i.e., the nodes of the meshes are irregularly arranged. Regular FD scheme

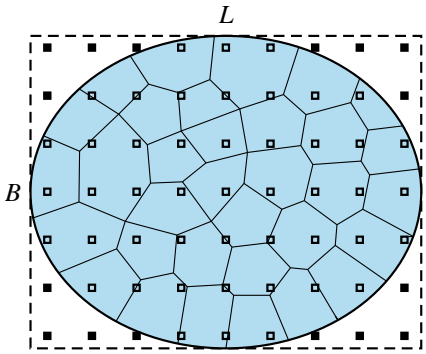

Fig. 6 Illustration of the finite difference scheme. The design domain D, discretized using polygonal elements, is represented by the ellipse and is enclosed within an imaginary *rectangular box* of length L and width B, represented by *dotted lines*. The *rectangular box* is filled with equidistant grid points, shown by *small squares*. For the grid points lying outside the ellipse (*solid squares*), the phase-field function value and sensitivity are assigned as zero, whereas, for other grid points, they are assigned the same value as the polygonal element in which they lie

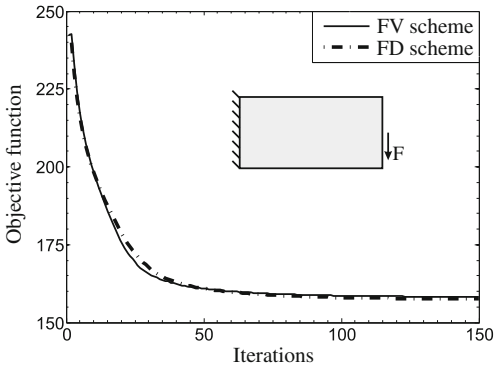

Fig. 8 Convergence history of the objective function for the cantilever beam problem of Fig. 7 for mesh discretization of 20,000 polygonal elements

based on (23) and (24) cannot be directly used to solve the Allen–Cahn equation on such a mesh with nodes (or element centers) as grid points. Thus, we propose the following approach to perform the FD, as illustrated by Fig. 6.

The ellipse represents the design domain D discretized using a polygonal mesh. The ellipse is enclosed within an imaginary rectangular box of length L and width B (represented by dotted lines). The rectangular box is filled with equidistant grid points (represented by small squares). The regular FD scheme can be applied on this structured grid. We need to resolve the phase-field function value on these grid points. First, a search routine needs to be performed to find the location of each grid point relative to the polygonal elements. For the grid points lying outside the design domain (solid squares), the phase-field function ϕ value is assigned as zero along with zero sensitivity $\bar{J}'(\phi)$. For other grid points, the phase-field function and sensitivity are taken to be the same as the corresponding values of the polygonal element inside which they lie. We have assumed that the phase-field function and the sensitivity are constant inside

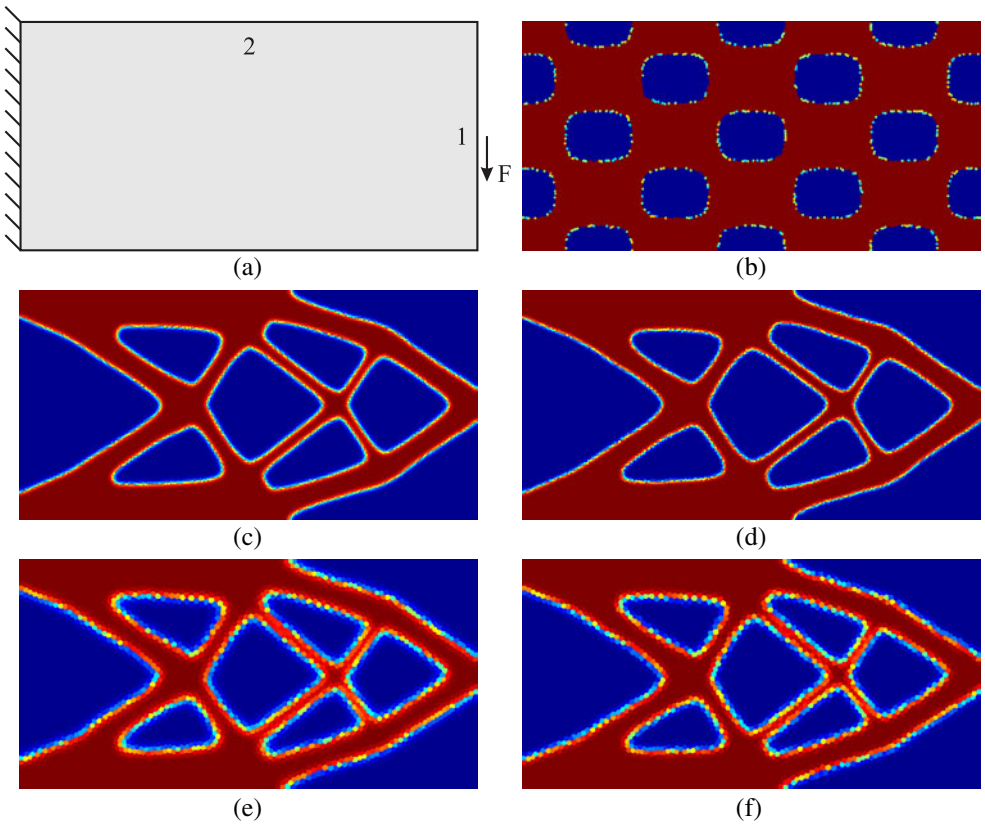

Fig. 7 Cantilever beam problem with load applied at the middle of right face. **a** Problem description. **b** Initial topology on 20,000 polygonal element mesh. Converged topologies on mesh discretization of 20,000 polygonal elements using **c** FV scheme, **d** FD scheme, and also on mesh discretization of 5,000 polygonal elements using **e** FV scheme, **f** FD scheme

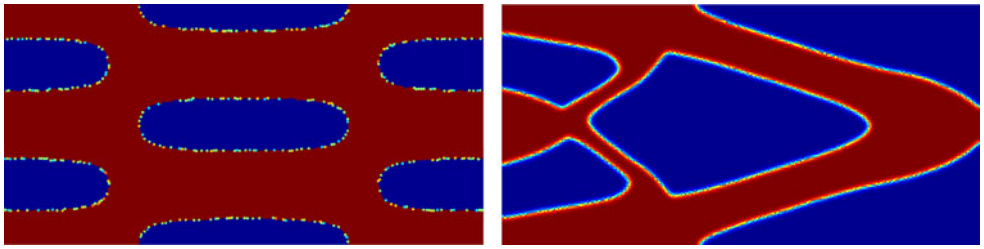

Fig. 9 Cantilever beam problem with a different initial topology. **a** Initial topology with 7 holes. **b** FV scheme

(a) (b)

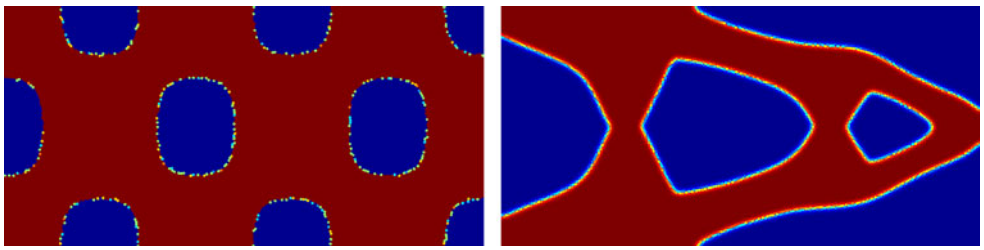

Fig. 10 Cantilever beam problem with another initial topology. **a** Initial topology with 9 holes. **b** FV scheme

(a) (b)

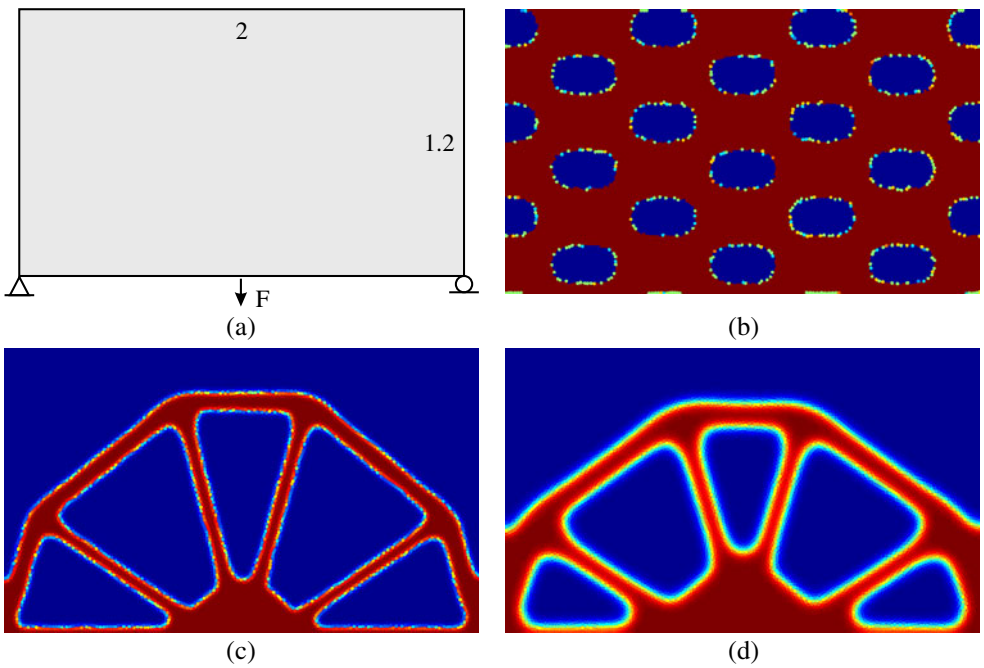

Fig. 11 Bridge problem solved using different diffusion coefficients κ for the FV approach. **a** Problem description. **b** Initial topology. **c** $\kappa = 2 \times 10^{-5}$. **d** $\kappa = 10 \times 10^{-5}$

(a) (b) (c) (d)

each element. After conducting an appropriate number of updates of the Allen–Cahn equation, the quantities computed on the structured grid need to be mapped backed to the polygonal mesh. We take the value of phase-field function for each element as the average of the values at all the grid points lying inside that element.

In this approach, we need at least one grid point to lie inside each polygonal element, which can be done by having a structured grid of sufficient refinement. Otherwise, the element's phase will not change throughout the optimization or, in other words, it will act as a "dead" element, resulting in an incorrect topology. To estimate the structured grid size, the number of grid points in the x and y direction are given by $\beta\sqrt{n_{\text{elem}}L/B}$ and $\beta\sqrt{n_{\text{elem}}B/L}$, respectively. Here n_{elem} is the number of polygonal elements in the finite element mesh and β is a multiplicative factor lying in the range $1.5 - 2$. The proposed finite difference scheme is heuristic in nature and possesses some approximations. The motivation behind its development is to provide an alternate scheme which gives a general idea of how the converged topologies should look like and thus can be used for estimating the accuracy of the results obtained from the finite volume scheme. In general, the CVT-based finite volume scheme, being more accurate, should be used.

4 Numerical examples

The use of polygonal finite elements makes it possible to perform topology optimization for complicated geometries. The mesh generator by Talischi et al. (2011) based on the implicit description of the design domain and centroidal Voronoi diagrams along with the FV/FD scheme makes this possible. In this section, we first illustrate some examples with conventional rectangular design domains for benchmark compliance minimization and linear compliant mechanism problems, followed by examples with non-conventional design domains. For all the examples, the parameters adopted are: $\eta = 10$, $k_{\min} = 10^{-4}$, Young's modulus E $= 1$, and Poisson's ratio $\nu = 0.3$. The time step Δt satisfies the CFL condition (Courant et al. 1928; Takezawa et al. 2010) and consistent units are employed. Note that the solution of the elasticity problem (1) is computationally expensive compared to one update step of the Allen–Cahn equation. Therefore, for fast convergence, after each FE iteration, we perform 20 FV/FD update steps of the Allen–Cahn equation (Takezawa et al. 2010; Allaire and Jouve 2004).

4.1 Cantilever beam problem

We first consider cantilever beam with load applied at the middle of right face. The objective is to obtain the stiffest configuration while using the least amount of material. The domain size is 2×1, discretized with 20,000 polygonal elements. The Lagrange multiplier λ is fixed at 95.

The diffusion coefficient is set to $\kappa = 1 \times 10^{-5}$ for all the examples in which the FD scheme is used to solve the Allen–Cahn equation. When the FV scheme is used to update the Allen–Cahn equation, the diffusion coefficient is taken as $\kappa = 2 \times 10^{-5}$, unless otherwise specified. The reason we chose a slightly higher diffusion coefficient for the FV approach is that the diffusion coefficient affects the thickness of diffuse interface and convergence is hindered if the

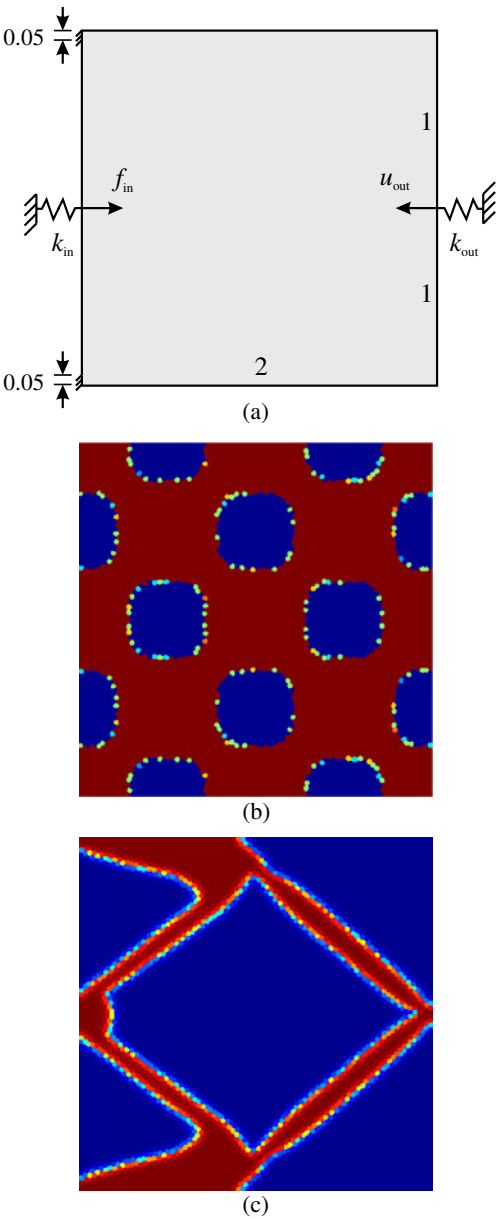

Fig. 12 Inverter problem on a polygonal mesh with 6,000 elements. **a** Problem description. **b** Initial topology. **c** Final configuration utilizing FV scheme

thickness is too small. A suitable value needs to be chosen based on level of mesh refinement. Finer meshes require a higher diffusion coefficient. In case of the FD scheme, the superimposed structured grid, on which FD operations are performed, is finer than the polygonal mesh thus a smaller value of diffusion coefficient is needed. The FV scheme is performed on the polygonal mesh itself, so a slightly larger diffusion coefficient is chosen. Figure 7b is chosen as the initial topology for the cantilever beam problem. Since the phase-field method can't generate holes, the initial topology needs to have enough holes so that it can converge to a meaningful topology. The resulting topologies, Fig. 7c (FV scheme is used to update Allen–Cahn equation) and Fig. 7d (FD scheme is used to update Allen–Cahn equation), are consistent with the ones seen in the literature (Allaire and Jouve 2004; Takezawa et al. 2010). For comparison purposes, we also solve the cantilever beam problem on a coarser mesh with 5,000 elements. All the parameters are chosen the same as before except $\kappa = 4 \times 10^{-5}$ for FD and $\kappa = 8 \times 10^{-5}$ for FV. Converged topologies (Figs. 7e and f) are similar to the ones on the finer mesh.

The convergence history of the objective function (5) for the above problem, for mesh discretization of 20,000 polygonal elements (Fig. 7c and d), is shown in Fig. 8. The FV scheme curve has a steeper slope, indicating a faster rate of convergence. This makes sense because the FD scheme is an approximate scheme which is less accurate than the FV scheme. But, both methods ultimately converge to similar objective function values.

The phase-field method converges to a local minimum, which, like other implicit function methods for topology optimization, such as level set method, is strongly dependent on the initial topology. This is due to the fact that this method can not generate holes in the domain—holes can only collapse. Converged topologies using the FV scheme are shown in Figs. 9b and 10b for the two other initial guesses of Figs. 9a and 10a, respectively. All parameters are kept the same as before.

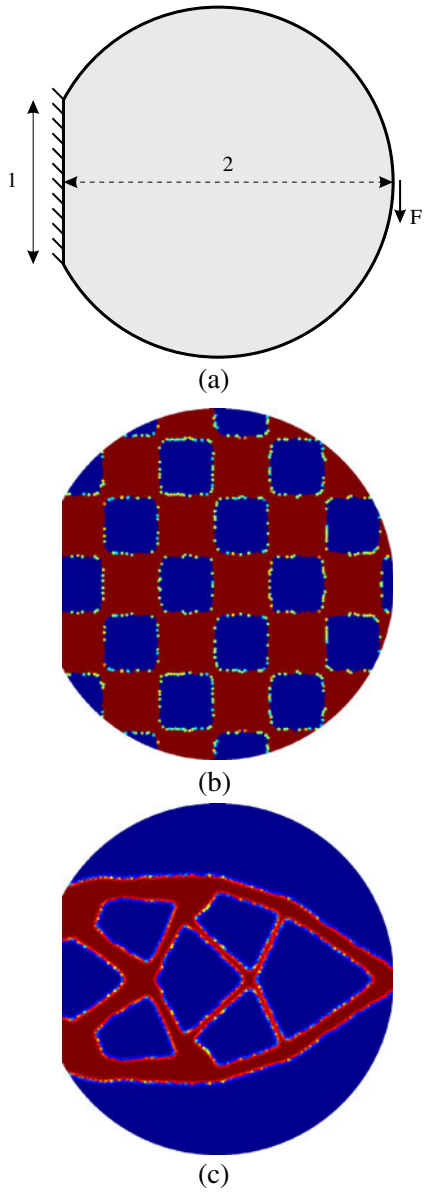

Fig. 13 Cantilever beam problem on a circular segment design domain. **a** Problem description. **b** Initial topology. **c** Converged topology using FV scheme

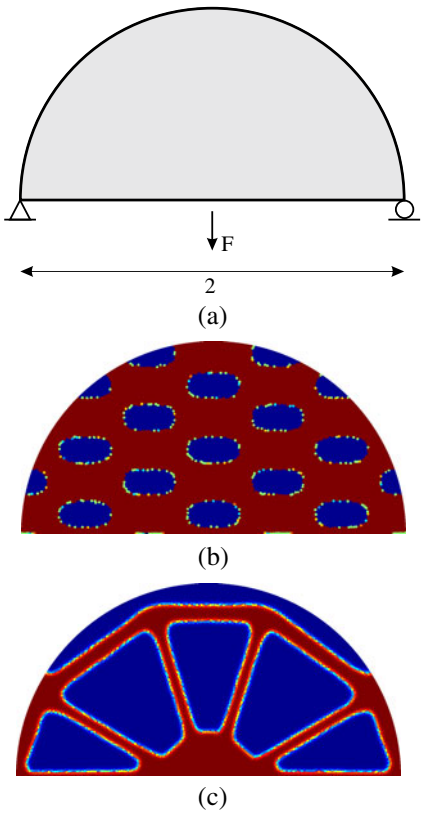

Fig. 14 Bridge problem on semi-circular design domain. **a** Problem description. **b** Initial topology. **c** FV scheme

4.2 Bridge problem

We next look at the bridge problem and study the influence of the diffusion coefficient, κ, on the optimization. The size of the design domain is a rectangle of size 2×1.2, discretized with 15,360 polygonal elements. The bottom corners are restrained by pin and roller supports, and a unit vertical force is applied at the middle of the bottom face (Fig. 11a). The objective (same as the last example) is to obtain the stiffest configuration while using the least amount of material. The parameter λ is chosen as 60 and $\kappa = 2 \times 10^{-5},\ 10 \times 10^{-5}$. Approximately 200 finite element iterations are needed for convergence of both the results, with the initial guess shown in Fig. 11b. The CVT based finite volume scheme is used to solve the evolution equation.

It is evident from Fig. 11c and d that κ influences the thickness of the diffuse interface. For $\kappa = 2 \times 10^{-5}$ and $\kappa = 10 \times 10^{-5}$, 28.2% and 46.3% elements, respectively, have phase-field values between 0.01 and 0.99 (Note that the design boundary $\partial\Omega$ lies in the region $0 < \phi(\boldsymbol{x}) < 1$). Thus, larger κ leads to a thicker interface. The current phase-field method implicitly possesses perimeter control effect which can be varied through κ. Bigger voids (larger perimeter) are obtained for lower κ (Fig. 11c) and smaller voids for larger κ (Fig. 11d). From this one may conclude that the smaller the value of κ, the better resolved the interface is. However, our numerical experiments using the current phase-field method have shown that, in order for the topologies to evolve smoothly, an appropriate value of κ has to be chosen for a particular mesh discretization. Hence, κ can not be indefinitely reduced to get a sharp interface. If a sharp, perfectly resolved interface is desired then an adaptive mesh refinement strategy near the interfaces may be adopted (cf. Feng and Wu 2008; Wallin et al. 2011) along with adaptive reduction in κ. Although pertinent, this investigation is beyond the scope of the current work.

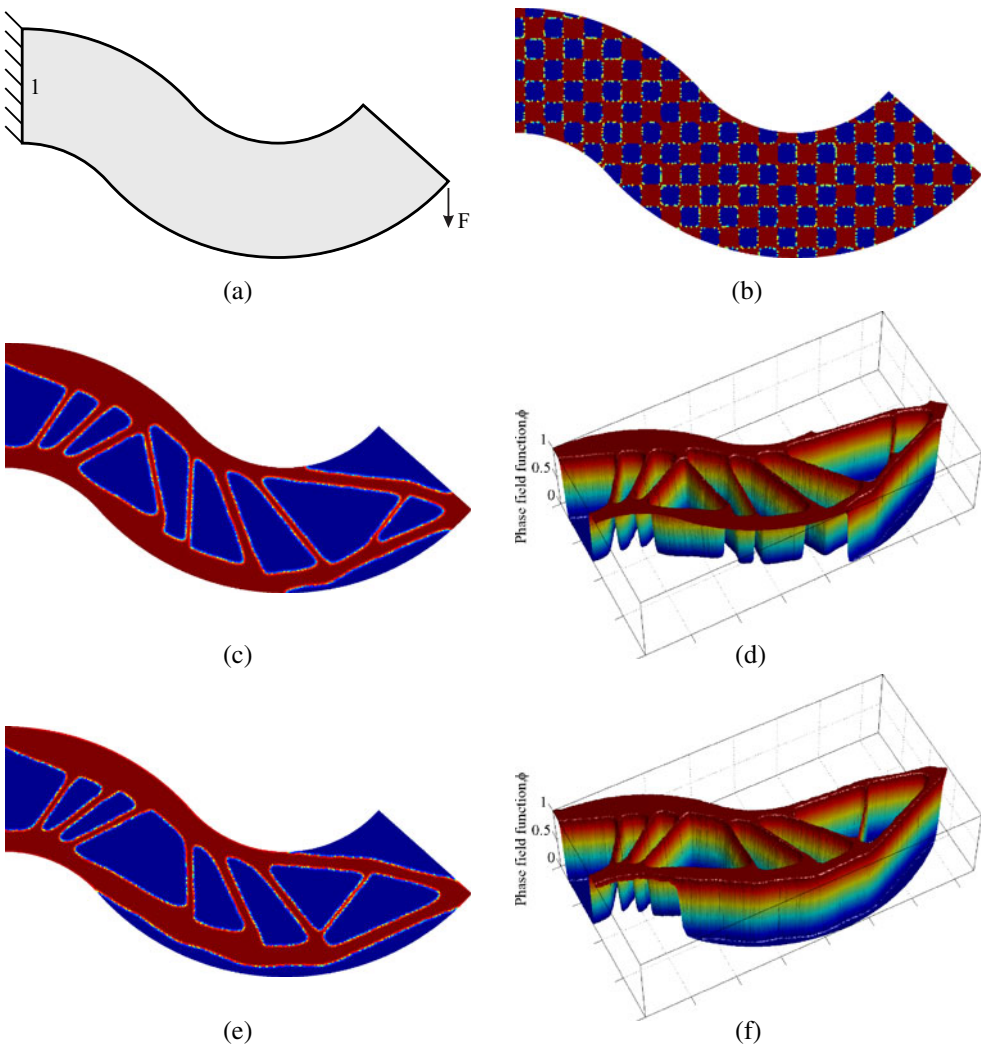

Fig. 15 Curved cantilever beam problem. **a** Problem description. **b** Initial topology. **c** FV scheme. **d** 3D visualization of (**c**). **e** FD scheme. **f** 3D visualization of (**e**)

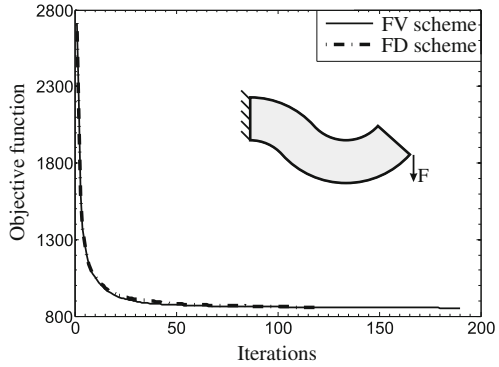

Fig. 16 Convergence history of the objective function for the curved cantilever beam problem of Fig. 15

4.3 Inverter problem on rectangular design domain

The phase-field method (discussed here) can also be used to solve compliant mechanism problems. We look at the classical inverter problem discussed in, for example, Bendsøe and Sigmund (2003). The problem is shown in Fig. 12a. The domain is a square of size 2×2, discretized using 6,000 polygonal elements. It is fixed on the top and bottom corners on the left face. The objective of the optimization problem is to maximize the output displacement u_{out}. Spring stiffnesses k_{in} and k_{out} are taken to have the same values of the components of the global stiffness matrix at the corresponding degrees of freedom. In order to obtain the sensitivities needed for the double well potential function, an adjoint system needs to be solved (see, for example, Bendsøe and Sigmund 2003). The FV scheme is used to solve the Allen–Cahn equation, and we set $\lambda = 0.02$ and $\kappa = 10 \times 10^{-5}$. For the initial guess of Fig. 12b, the converged configuration is shown in Fig. 12c, which is similar to Fig. 5.5 of Bendsøe and Sigmund (2003).

4.4 Cantilever beam problem on a circular segment domain

The benchmark example of cantilever beam problem, with vertically downward load applied on the midpoint of the right face, is now solved on a design domain in the shape of a circular segment (Fig. 13a). Figure 13b is chosen as the initial guess. The design domain is a symmetric polygonal mesh (about the horizontal axis) with 12,800 elements. Figure 13c shows the converged topology, utilizing the FV scheme and $\lambda = 95$. Although the design domain chosen here is different from the conventional one, the converged

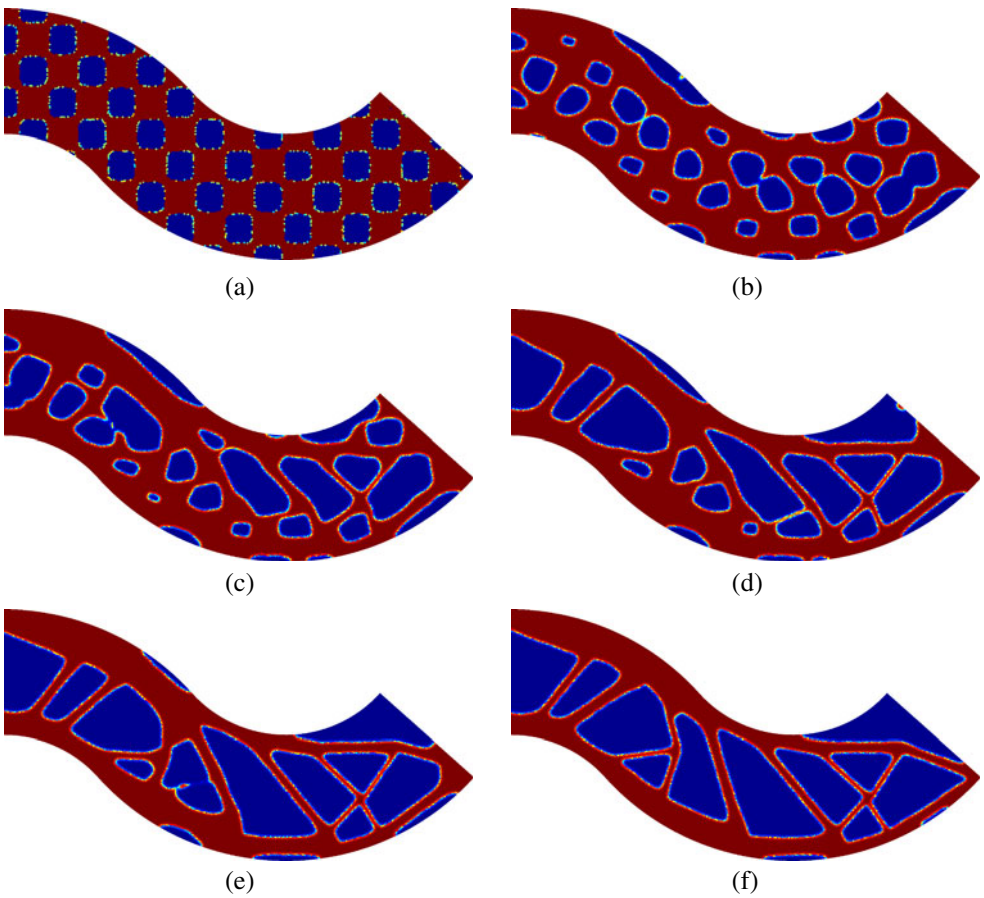

Fig. 17 Evolution of the topology for the curved cantilever beam problem using FV scheme for a different initial guess. **a** Initial topology. **b** Iteration 13. **c** Iteration 19. **d** Iteration 29. **e** Iteration 51. **f** Converged topology

topologies are similar to the ones with rectangular design domains (cf. Figs. 13 and 7).

4.5 Bridge problem on a semi-circular domain

Next, we consider the bridge problem on a semi-circular design domain (Fig. 14a). The boundary conditions are the same as the ones for the bridge problem on a rectangular domain discussed before. The polygonal mesh used to discretize the design domain consists of 11,000 elements, and λ is chosen as 60. The optimization is performed with Fig. 14b as the initial guess and it converges to Fig. 14c for the FV updating scheme, which resembles the result obtained on the rectangular domain (Fig. 11c).

4.6 Curved cantilever beam problem

In the literature, rectangular/cuboidal design domains have been the preferred domain shapes for topology optimization. To depart from this trend, consider the problem of cantilever beam on a doubly curved design domain (Fig. 15a). The domain is discretized using 20,000 polygonal elements. The Lagrange multiplier λ is chosen as 250. Converged topologies for the chosen initial design, Fig. 15b, are shown in Fig. 15c for the FV scheme and Fig. 15e for the FD scheme. Figure 15d and f are the 3D visualizations of the corresponding phase-field functions.

Figure 16 shows the convergence history of the objective function (5) for the above curved cantilever beam problem (Fig. 15). Although both FV and FD schemes seem to converge to similar objective function values, the converged topologies are somewhat different. As stated before, the FD scheme involves more approximation than the FV scheme (refer to Section 3.2). In the FD scheme, the phase-field function values at the grid points (lying inside the design domain) are assumed to be the same as the corresponding value of the polygonal element inside which they lie. This leads to inefficient evaluation of $\nabla^2\phi$ in (12) which results in a different converged topology when compared to the FV scheme. This inefficiency reduces as the mesh becomes finer. The differences between the schemes are amplified because of the unstructured nature of the polygonal meshes used here. When structured quad elements are used and only one grid point lies inside each quad for the FD scheme, then both methods produce exactly the same result.

To demonstrate the previously stated fact that, in the phase-field method, converged topologies depend on the initial guess, we solved the doubly curved cantilever problem on a different initial guess (Fig. 17a). Figures 17b–f show the evolution of topologies over time for the new initial guess.

4.7 Inverter problem on circular segment domain

Finally, we consider the inverter problem on a non-rectangular design domain. The domain is in the shape of a circular segment, discretized into 6,000 polygonal elements. All the other parameters are kept same as the inverter problem on the rectangular domain discussed before (cf. Fig. 12). The problem description is shown in Fig. 18a. The design domain of circular segment chosen here, although non traditional, has similar boundary and loading conditions to the traditional example on a rectangular domain (see Bendsøe and Sigmund 2003). The converged topology

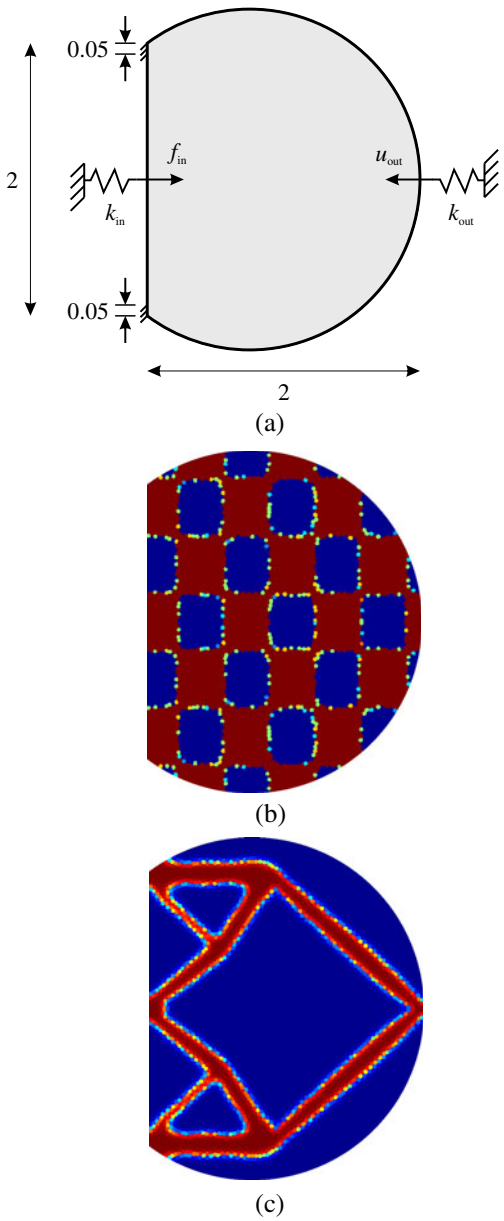

Fig. 18 Inverter problem on a circular segment design domain. **a** Problem description. **b** Initial topology. **c** FV updating scheme

(Fig. 18c for FV updating schemes) is similar to the one with rectangular design domain (cf. Figs. 18c and 12c).

5 Concluding remarks

In the current paper, we employ a fully unstructured polygonal finite element based mesh to implement a phase-field method for structural topology optimization. The polygonal meshes are based on Voronoi tessellations (Talischi et al. 2011) which not only facilitate non-mesh biased designs but also provide greater flexibility in discretizing non-Cartesian design domains. A CVT-based finite volume method is used to solve the phase-field evolution equation (Allen–Cahn PDE) on unstructured polygonal meshes. An alternate approach using a finite difference scheme is also presented to solve the phase-field equation.

Phase-field methods, similar to the one discussed in this work, bear a resemblance to the level-set methods in the sense that the topologies are represented in terms of implicit functions and evolved using certain governing PDEs. The most characteristic difference between the two is the fact that in level-set methods the interface is explicitly defined and tracked ($\phi = 0$ contour), whereas, in the phase-field approach the interfaces have a finite thickness (requiring no tracking of the interfaces). In the phase-field method, topologies are evolved by solving the governing equations over the complete design domain without any prior knowledge of location of phase boundaries. In order to resolve the phase interfaces (obtaining a 0-1 design) an adaptive mesh refinement strategy or other alternative approaches may be used, e.g. Sun and Beckermannn (2007).

The present approach has been used to solve 2D compliance minimization and compliant mechanism problems on complicated design domains. It can also be used to solve structural optimization problems such as eigenvalue problems, design dependent load problems, and nonlinear elasticity problems on any desired design domain. For this purpose, sensitivities need to be evaluated, for each particular objective function, to define the double well potential function. Since the phase-field method employed in this work has no embedded hole generation mechanism, the final topologies are greatly influenced by the initial shapes. Topological derivatives (Eschenauer and Schumacher 1994; Sokolowski and Zochowski 1999; Céa et al. 2000) can be used to alleviate this issue. In future work, we plan to extend our scheme to 3D using polyhedral meshes, and explore possible applications such as craniofacial segmental bone replacement in the field of biomedical engineering (Sutradhar et al. 2010; Nguyen et al. 2010, 2011). The work by Wicke et al. (2007) and Martin et al. (2008) on polyhedral finite elements can be useful for that purpose. In closing, we remark that phase-field method, with sharpness control of diffuse interfaces, offers an attractive framework for phononic metamaterial cloaking device designs (see Pendry et al. 2006).

Nomenclature

$\boldsymbol{u}$	Admissible displacement field satisfying equilibrium
$\boldsymbol{\varepsilon}$	Strain field
$\boldsymbol{f}$	Body force
$\boldsymbol{g}$	Surface loads
$\boldsymbol{C}$	Elasticity tensor
$\boldsymbol{C}^*$	Effective elasticity tensor
ϕ	Phase-field function
Ω	Admissible design for the optimization problem
D	Working domain which contains all the admissible shapes Ω
Ω_1	Solid phase domain
Ω_0	Void phase domain
ξ	Diffuse interface
$J_i(\phi)$	Objective function
$\bar{J}(\phi)$	Reformulated objective function
$\bar{J}'(\phi)$	Sensitivity of the reformulated objective function
λ	Lagrangian multiplier used to reformulate the objective function
k_{in}	Input spring stiffness
k_{out}	Output spring stiffness
u_{out}	Output displacement
$\mathcal{P}$, $\mathcal{Q}$	Set of natural neighbors
N_i	Laplace shape function
α_i	Laplace weight function
s_i	Length of the common Voronoi edge associated with point q and node q_i
S_i	Length of the common Voronoi edge associated with the points p and p_i
h_i	Distance between point q and node q_i
H_i	Distance between the points p and p_i
$k_{\min}$	Scaling factor to determine lower limit of $\boldsymbol{C}^*$
$f(\phi)$	Double well potential function
η	Scaling constant
κ	Diffusion coefficient
$\boldsymbol{n}$	Normal to the edge of a Voronoi cell
D_p	Domain of the Voronoi cell centered at p
Γ_p	Boundary of the domain D_p
V_p	Area of the Voronoi cell centered at p
ϕ_p^n	ϕ for the nth iteration at the center of the Voronoi cell associated with p
$\phi_{i,j}^n$	ϕ for the nth iteration at the grid point located at $\boldsymbol{x}_{i,j}$
n_{elem}	Number of polygonal elements in the finite element mesh

L	Length of the imaginary rectangular grid circumscribing the design domain D
B	Width of the imaginary rectangular grid circumscribing the design domain D
β	Parameter to control structured FD mesh refinement
Δt	Time step
Δx	Distance between grid points in x direction
Δy	Distance between grid points in y direction

References

Allaire G, Jouve F (2004) Structural optimization using sensitivity analysis and a level-set method. J Comput Phys 194:363–393

Allen SM, Cahn JW (1979) A microscopic theory for antiphase boundary motion and its application to antiphase domain coarsening. Acta Metall 27:1085–1095

Aranson IS, Kalatsky VA, Vinokur VM (2000) Continuum field description of crack propagation. Phys Rev Lett 85(1):118–121

Bendsøe MP (1989) Optimal shape design as a material distribution problem. Struct Optim 1:193–202

Bendsøe MP, Kikuchi N (1988) Generating optimal topologies in structural design using a homogenization method. Comput Methods Appl Mech Eng 71(2):197–224

Bendsøe MP, Sigmund O (1999) Material interpolation schemes in topology optimization. Arch Appl Mech 69(9–10):635–654

Bendsøe MP, Sigmund O (2003) Topology optimization—theory, methods and applications. Springer, New York

Bolander JE, Saito S (1998) Fracture analysis using spring networks with random geometry. Eng Fract Mech 61:569–591

Bourdin B (2001) Filters in topology optimization. Int J Numer Methods Eng 50(8):2143–2158

Bourdin B, Chambolle A (2003) Design-dependent loads in topology optimization. ESAIM—Control Optim Calc Var 9:19–48

Burger M, Stainko R (2006) Phase-field relaxation of topology optimization with local stress constraints. SIAM J Control Optim 45(4):1447–1466

Caginalp G (1986) An analysis of a phase field model of a free boundary. Arch Ration Mech Anal 92(3):205–245

Cahn JW, Hillard JE (1958) Free energy of a nonuniform system. I. Interfacial energy. J Chem Phys 28:258–267

Céa J, Garreau S, Guillaume P, Masmoudi M (2000) The shape and topological optimizations connection. Comput Methods Appl Mech Eng 188(4):713–726

Courant R, Friedrichs KO, Lewy H (1928) Über die partiellen Differenzengleichungen der mathematischen Physik. Math Ann 100(1):32–74

Cuthill E, McKee J (1969) Reducing the bandwidth of sparse symmetric matrices. In: Proceedings of the 24th national conference. ACM Press, New York, pp 157–172

Diaz AR, Sigmund O (1995) Checkerboard patterns in layout optimization. Struct Multidisc Optim 10(1):40–45

Eschenauer H, Schumacher A (1994) Bubble method for topology and shape optimization of structures. Struct Optim 8(1):42–51

Feng X, Wu H (2008) A posteriori error estimates for finite element approximations of the Cahn–Hilliard equation and the Hele–Shaw flow. J Comput Math 26(6):767–796

Ghosh S (2011) Micromechanical analysis and multi-scale modelling using the Voronoi cell finite element method. CRC Press, Boca Raton, FL

Ghosh S, Mukhopadhyay SN (1991) A two-dimensional automatic mesh generator for finite element analysis for random composites. Comput Struct 41(2):245–256

Guest JK, Prevost JH, Belytschko T (2004) Achieving minimum length scale in topology optimization using nodal design variables and projection functions. Int J Numer Methods Eng 61(2): 238–254

Kobayashi R (1993) Modeling and numerical simulations of dendritic crystal growth. Phys D: Nonlin Phenom 63(3–4):410–423

Lloyd S (1982) Least squares quantization in PCM. IEEE Trans Inf Theory 28(2):129–137

March R (1992) Visual reconstructions with discontinuities using variational methods. Image Vis Comput 10:30–38

Martin S, Kaufmann P, Botsch M, Wicke M, Gross M (2008) Polyhedral finite elements using harmonic basis functions. Comput Graph Forum 27(5):1521–1529

Nguyen TH, Paulino GH, Song J, Le CH (2010) A computational paradigm for multiresolution topology optimization (MTOP). Struct Multidisc Optim 41(4):525–539

Nguyen TH, Song J, Paulino GH (2011) Single-loop system reliability-based topology optimization considering statistical dependence between limit-states. Struct Multidiscipl Optim 44(5):593–611

Osher S, Fedkiw R (2003) Level set methods and dynamic implicit surfaces. Springer, New York

Osher S, Sethian JA (1988) Front propagating with curvature-dependent speed: algorithms based on Hamilton–Jacobi formulations. J Comput P 79:12–49

Paulino GH, Menezes IFM, Gattass M, Mukherjee S (1994a) Node and element resequencing using the Laplacian of a finite element graph. Part I: General concepts and algorithm. Int J Numer Methods Eng 37(9):1994

Paulino GH, Menezes IFM, Gattass M, Mukherjee S (1994b) Node and element resequencing using the Laplacian of a finite element graph. Part II: Implementation and numerical results. Int J Numer Methods Eng 37(9):1531–1555

Pendry PD, Schurig D, Smith DR (2006) Controlling electromagnetic fields. Science 312:1780–1782

Pingen G, Waidmann M, Evgrafov A, Maute K (2010) A parametric level-set approach for topology optimization of flow domains. Struct Multidisc Optim 41(1):117–131

Rozvany GIN, Querin OM, Gaspar Z, Pomezanski V (2003) Weight-increasing effect of topology simplification. Struct Multidisc Optim 25(5–6):459–465

Rozvany GIN, Zhou M, Birker T (1992) Generalized shape optimization without homogenization. Struct Multidisc Optim 4(3–4):250–252

Sethian JA (1999) Level-set methods and fast marching methods: evolving interfaces in computational geometry, fluid mechanics, computer vision and materials science. Cambridge University Press, Cambridge, UK

Sigmund O, Peterson J (1998) Numerical instabilities in topology optimization: a survey on procedures dealing with checkerboards, mesh-dependencies and local minima. Struct Optim 16(1):68–75

Sokolowski J, Zochowski A (1999) On the topological derivatives in shape optimization. SIAM J Control Optim 37:1251–1272

Sukumar N, Tabarraei A (2004) Conforming polygonal finite elements. Int J Numer methods Eng 61(12):2045–2066

Sun Y, Beckermann C (2007) Sharp interface tracking using the phase-field equation. J Comput Phys 220(2):626–653

Sutradhar A, Paulino GH, Miller MJ, Nguyen TH (2010) Topology optimization for designing patient-specific large craniofacial segmental bone replacements. Proc Natl Acad Sci 107(30):13222–13227

Suzuki K, Kikuchi N (1991) A homogenization method for shape and topology optimization. Comput Methods Appl Mech Eng 93(3):291–318

Takezawa A, Nishiwaki S, Kitamura M (2010) Shape and topology optimization based on the phase field method and sensitivity analysis. J Comput Phys 229:2697–2718

Talischi C, Paulino GH, Pereira A, Menezes IFM (2010) Polygonal finite elements for topology optimization: A unifying paradigm. Int J Numer Methods Eng 82:671–698

Talischi C, Paulino GH, Pereira A, Menezes IFM (2011) PolyMesher: A general-purpose mesh generator for polygonal elements written in MATLAB. Struct Multidisc Optim 45(3):309–328

Vasconcellos JFV, Maliska CR (2004) A finite-volume method based on Voronoi discretization for fluid flow problems. Numer Heat Transf B 45:319–342

Wallin M, Ristinmaa M, Askfelt H (2012) Optimal topologies derived from a phase-field method. Struct Multidisc Optim 45(2):171–183

Wang MY, Wang X, Guo D (2003) A level-set method for structural topology optimization. Comput Methods Appl Mech Eng 192:227–246

Wang MY, Zhou S (2004a) Phase field: A variational method for structural topology optimization. Comput Model Eng Sci 6(6):547–566

Wang MY, Zhou S (2004b) Synthesis of shape and topology of multimaterial structures with a phase-field method. J Comput-Aided Mater Des 11:117–138

Warren JA, Kobayashi R, Lobkovsky AE, Carter WC (2003) Extending phase field models of solidification to polycrystalline materials. Acta Mater 51(20):6035–6058

Wicke M, Botsch M, Gross M (2007) A finite element method on convex polyhedra. Comput Graph Forum 26(3):355–364

Yip M, Mohle J, Bolander JE (2005) Automated modeling of three-dimensional structural components using irregular lattices. Comput-Aided Civil Infrastruct Eng 20(6):393–407

Zhou S, Wang MY (2007) Multimaterial structural topology optimization with generalized Cahn-Hilliard model of multiphase transitions. Struct Multidiscipl Optim 33:89–111